Molecular Dynamics Studies of the Phase Transitions of Homopolymers of *p*-Hydroxybenzoic Acid

M. Nolan and J. C. Greer*

National Microelectronics Research Centre, University College, Lee Maltings, Prospect Row, Cork, Ireland

Received: January 7, 1999; In Final Form: May 10, 1999

Studies of liquid crystals composed of the homopolymer of *p*-hydroxybenzoic acid are presented based upon force-field (FF) and molecular dynamics (MD) methods. Structural data has been extracted from MD simulations to characterize the nature of the high-temperature phase transitions which have been experimentally identified for these polymers. Discontinuities in the isobaric heat capacity calculated as a function of temperature are taken to be signatures for the various phase transitions that HBA undergoes. Typically, the structural transitions are predicted by the simulations at temperatures agreeing within 10 to 15 °C of the transitions observed in differential scanning calorimetry measurements. Variations in crystallographic lattice constants determined from X-ray diffraction patterns are reproduced well by the simulations. The transition from an orthorhombic unit cell in a low-temperature phase (below 340 °C) to a pseudohexagonal unit cell at higher temperatures is experimentally observed for HBA homopolymers and has also been observed in the course of these simulations. In general, the simulations and methods applied are suitable for a description of the occurrence of phase transitions within these novel liquid crystal materials, are useful for characterization of the packing and relative orientations between chains, as well as providing a detailed description of the reorganization of the phenyl rings and ester linkages along the chain axes.

1. Introduction

Liquid crystal polymers (LCPs) of *p*-hydroxybenzoic acid (HBA) have been extensively studied[1−8] and copolymers of HBA and 1,6-hydroxynaphthoic acid (HNA) are of substantial commercial interest. Studies of the homopolymer of HBA have been primarily concerned with (i) determination of the temperatures at which HBA undergoes phase transitions[1−6] and (ii) the attendant structural changes which HBA undergoes at these phase transitions.[1−6]

In this work, force-field (FF)[9] calculations and molecular dynamics (MD) simulations[10,11] are performed to calculate the temperatures at which phase transitions occur and to analyze at a molecular level the structural changes which occur at the phase transitions. This work is the first study, of which we are aware, applying MD methods to directly investigate the structural phase transitions of polyester LCPs. It is well established that the structures of copolymers formed from HBA and HNA are similar to those of the parent homopolymers at room temperature and the nature of the phase transitions the systems undergo are related.[8] Hence studies of HBA, while being of intrinsic interest, also serve as a basis for further general studies of ester-linked aromatic copolymers.

An early synthesis of poly-HBA is that of Economy et al.[1] in 1976, who also studied the room-temperature structure using X-ray powder diffraction. The room-temperature structure of HBA was also studied by Lieser[2] using X-ray and electron diffraction and more recently by Yoon et al.[7] using X-ray powder diffraction. The unit cell of HBA was found to be orthorhombic and composed of two dimer chains, has the following lattice constants:[7] $a = 7.42$ Å, $b = 5.67$ Å, and $c = 12.45$ Å and a density of $\rho = 1.48$ g/cm^3. The structure of the room-temperature unit cell is such that the rings are staggered along the *c*-direction and the carbonyl groups of the ester linkage are staggered by 120°. The deduced packing in the HBA homopolymer is such that edge-face interactions are dominant.[7] The HBA dimer depicting the ester links by which the HBA homopolymers are constructed is given in Figure 1: three structurally important bonds E, F, and G about which torsional motion dictates chain geometry are also labeled within the figure.

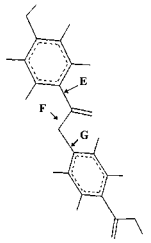

Figure 1. Dimer of HBA, with ester torsions E, F, and G shown.

There occurs for solid HBA a first phase transition at 340 °C, which has been determined by differential scanning calorimetry (DSC).[1−4,6] The structure of HBA at this and the higher temperature phase transitions has been studied using X-ray and electron diffraction, wide-angle X-ray spectroscopy (WAXS) and model calculations.[1−6] At this first phase transition, the major structural changes are the following: (i) a significant increase in lattice constant *a*,[2−4,6,8] giving a significant increase in the cell volume, (ii) a slight decrease in lattice constant *b*,[2−4,6] and (iii) a change in the space lattice.[6,12] The change in lattice symmetry was first shown in ref 2 where Lieser showed that at this transition the packing in the *ab* plane becomes pseudohexagonal—an orthorhombic unit cell whereby the chains are arranged on a hexagonal net. From the diffraction pattern obtained in this work and later work of Economy et al.[4] and Yoon et al.,[6] it was shown that the unit cell had to be indexed as orthorhombic, due to the absence of both the 211[6] and 200[4] reflections, with lattice constants $a = 9.2$ Å, $b = 5.3$ Å, and $c = 12.4$ Å. The absence of the latter reflection is associated with

* Author to whom correspondence should be addressed.

10.1021/jp990101n CCC: $18.00
Published on Web 07/27/1999

a sharp change in a.[4] However since the relationship $a = \sqrt{3}b$ holds, the molecules are positioned on a hexagonal net. Hanna and Windle[3] and Kricheldorf and Schwarz[5] attributed the increase in a to increased rotational freedom of the phenylene rings around the 1,4 axis of the phenyl ring, without the rings acquiring full rotational freedom. In the work of Flores et al.[12] it is shown that as the temperature is increased, the value of the lattice constant γ changes from 90° to 120° at the phase transition. Their work indicates that the unit cell changes from an orthorhombic to hexagonal unit cell.

A second phase transition occurs at 430 °C.[5,6] The structure of HBA at this second high-temperature phase transition has not been as well characterized in comparison to the structures accompanying the transition at 340 °C. Yoon et al. have shown that the lattice constants a and b take the values $a = 9.35$ Å and $b = 5.3$ Å[6] for this structure at 430 °C, i.e., the lattice constants change very little. Kricheldorf and Schwarz[5] studied this high-temperature transition using micrographs and WAXS. The WAXS measurements showed that the pseudohexagonal chain packing formed at the 340 °C transition persists past this second phase transition. It was concluded from their results, that this transition is not the melting point and the origin of this transition was attributed to more rotational freedom for the phenyl rings, but without them ever gaining full rotational freedom.[5]

In 1980, Jackson reported a phase transition for HBA at 610 °C.[13] This was stated to be the melting point. However, no DSC trace was presented. Kricheldorf and Schwarz[5] stated that this interpretation is incorrect and that the transition at 510−530 °C is actually the melting point. This transition was characterized as the melting point using a combination of IR spectroscopy, microscopy and WAXS measurements. The samples heated to 550 °C were found to be amorphous, had lost their crystalline shape, and looked like molten fibers. Transesterification reactions were reported, which signifies decomposition of the sample in temperatures above 500 °C.

In contrast to the experimental characterizations, there has been relatively little theoretical work performed for these LCPs. Oligimers of HBA (dimers and tetramers) were studied by Huth et al. using molecular dynamics.[14] However their work is concerned with the calculation of the liquid crystalline order parameter for HBA oligimers at two temperatures. In contrast to their work we study infinite polymer chains as a result of the periodic boundary conditions and also the thermal behavior over a wide range of temperatures in order to characterize the phase transitions. Fougler and Rutledge studied the two high-temperature phases of HBA at 335 and 430 °C using Monte Carlo methods within the canonical (NVT) ensemble.[15] It was decided to use an MC procedure because the time scale for the motion of the phenyl rings was anticipated to be several orders of magnitude beyond the reach of an MD simulation. In many respects, the present study complements their Monte Carlo work. The use of the canonical ensemble in the Monte Carlo simulations precludes any volume changes, whereas no such restriction applies to the MD simulations presented here. This allows for the polymers to be studied over a range of temperatures without constraining the simulation to a particular unit cell or crystal lattice. The phase transitions, in particular the first phase transition at 340 °C, appear to be primarily governed by the motion of the ester torsions and not the rings, which will be discussed in this work, and so MD appears to be suitable for studies of poly-HBA. In both refs 14 and 15 the bond lengths and angles are kept fixed, whereas no such constraints are applied in this work.

TABLE 1: Lattice Constants *a* and *b* and Volume for the Energy Minimized Simulation Cells of HBA As Studied in This Work[a]

HBA simulation cell length	*a*/Å	*b*/Å	V/Å^3
dimer	7.85	5.28	132
trimer	7.86	5.38	134
tetramer	8.52	5.27	143
hexamer	8.27	5.23	138

[a] The simulation cells are two chains of the given number of monomers per simulation cell.

From the above discussion, there are some outstanding issues which we address through the use of MD simulation. These issues are the following. (i) It has been proposed that the motion of the phenyl rings around their 1,4-axes is responsible for the first two phase transitions.[5,8] However, might there also be a freeing up of the motion of the ester torsions in addition to this ring motion? (ii) Phenyl ring flips are again postulated to occur at temperatures greater than 500 °C. Does this actually occur and is there any other accompanying motion which occurs at these high temperatures? (iii) In the work of Flores et al.,[12] it was shown that the lattice constant γ changes from 90° to 120° at the first phase transition. However, X-ray and electron diffraction studies show clearly that an orthorhombic unit cell (with hexagonal packing) with $\gamma = 90°$ is present above the first phase transition.[2,6] These appear to be two different structures and this begs the question: which provides a better description of HBA above the first phase transition? From the work of Fougler and Rutledge[15,16] we use the pseudohexagonal unit cell for the study of the second and higher phase transitions.

2. Computational Methods

The first step in the calculations is the construction of a simulation cell. The initial lattice constants and packing are taken from the experimental studies of ref 7. All calculations presented use a two-chain simulation cell. The choice of a two-chain cell, although introducing a high degree of crystallinity, is justified by crystallographic data and the simulation results themselves. The periodic boundary conditions used in the simulations presented here introduce a high degree of order; to allow the system to deviate from a regular crystalline structure requires the introduction of more chains per simulation cell and longer chain lengths within the simulation cell. However, the computational time is directly proportional to the number of atoms per simulation cell. Hence the choice of simulation cell in these simulations is a compromise between the ideal repeat distance in any direction and the computational time needed for the simulation. To investigate this effect, simulation cells with two (dimer), three (trimer), four (tetramer), and six (hexamer) monomers per chain were studied in order to to investigate the effects introduced by cell constraints.

Lattice constants for the cells composed of dimer, trimer, tetramer, and hexamer repeat units studied in this work are given in Table 1. These simulation cells are minimized structures at $T = 0$ K. We note the differing value of lattice constant a for each of these structures. Presumably, this is related to the fact that a longer chain is not as linear as a smaller chain and with the phenyl edge-to-face packing present this causes the a dimension to be larger for a longer simulation cell.

HBA has a high degree of two- and three-dimensional order and intermolecular registration within the unit cell. To simulate this, the chains are oriented parallel to the c-direction so that a degree of crystallinity, both along a chain and perpendicular to the chain axis, is present in the simulations from the outset.

Also a high degree of axial registration is present. The introduction of order to the system in this way reduces the time needed to bring the system to equilibrium. However, a system that is too ordered (crystalline) does not represent the true structure of these LCPs as some measure of disorder, from the very nature of LCPs, must be present; see also ref 14.

Once a simulation cell has been constructed, periodic boundary conditions are applied and the periodic structure is then minimized without constraints using the PCFF force field.[9] The cutoff for Coulomb and van der Waals terms is a cubic spline method and the spline-on and spline-off distances are 8.0 Å and 8.5 Å, respectively. For use in the MD studies, atomic charges were obtained from electrostatic potential (ESP) charges fit to the charge density distribution calculated from a geometry optimization of the HBA trimer using the B-LYP[17,18] DFT functional, with a 6-31G* basis set[19] and a medium grid,[20] as implemented in Turbomole[21] within InsightII from MSI.[22] All force-field calculations and molecular dynamics simulations were carried out within the Cerius[2] set of programs from MSI.[22]

All minimized structures resulted in an orthorhombic unit cell in agreement with the experimental room-temperature structure determinations.[2,7] The minimized structure is then used as the initial configuration for subsequent MD simulations. To prepare the system, an 850 ps MD run is carried out at a temperature of 177 °C, chosen to be well below the first high-temperature phase transition yet at a sufficiently high temperature to allow equilibration of the system along the chain axes. Relaxation runs were also carried out at a set of temperatures, 27, 202, and 277 °C, to study the effect on the simulations resulting from different initial conditions. The equilibration run at 27 °C is found to effect the results of the simulations if the system is not further equilibrated at a higher temperature, e.g. 177 °C. The reason for this is that at low temperatures the molecular motion necessary to equilibrate the system cannot occur. For the higher-temperature relaxation runs, subsequent MD simulations were found to be insensitive to initial conditions. Starting from a relaxed configuration, a further 75 ps simulation is performed at 177 °C and further simulations are carried out at temperature intervals of of 25 °C (or in some instances, 50 °C) up to the first phase transition, T_{PT1}. Thermodynamical averages are performed using the 65 ps intervals with the initial 10 ps at each new temperature discarded as equilibration time.

Subsequent high-temperature simulations were conducted by constructing a hexagonal and pseudohexagonal structure corresponding to the experimental cell geometry[6,12] with the initial geometry taken from a structure obtained at T_{PT1}. The initial relaxation simulation is carried out for 850 ps, and 75 ps simulations are carried out up to the second phase transition. The structure is then further relaxed above this phase transition, and 75 ps simulations are again carried out up to the third transition point.

The MD simulations are conducted within the NPT−*N*, constant number of particles, *P*, constant pressure; *T*, constant temperature−ensemble. The pressure is held constant using the Parrinello−Rahman method.[23] The cell mass pre-factor, *Q*, from this method was assigned a value of 10. The temperature is held constant using the Nosé method as modified by Hoover to remove time scaling.[24,25] For integration of the equations of motion the Verlet leapfrog algorithm[26] is used with a time step of 1 fs. Configurations are saved every 0.01 ps for calculation of the isobaric specific heat capacity, lattice constants, and various geometry distributions for use in determining the molecular motion occurring at the phase transitions. The initial assignment of velocities is selected randomly from a Maxwell−Boltzmann distribution at the desired temperature.

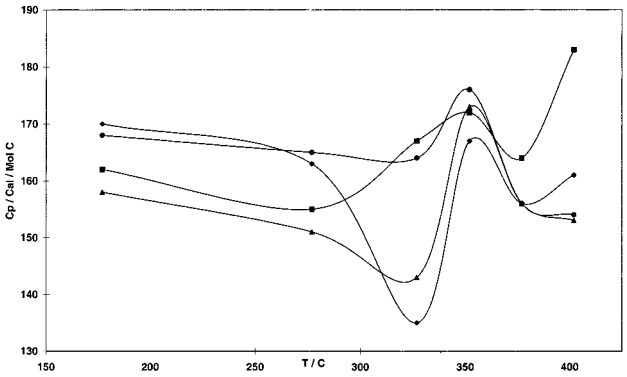

Figure 2. Calculated isobaric specific heat capacity against simulation temperature (up to T_{PT1}) for HBA dimer (diamonds), trimer (squares), tetramer (triangles), and hexamer (circles) simulation cells. For each of these structures a phase transition is seen to occur at 350 °C. The curve is to guide the eye.

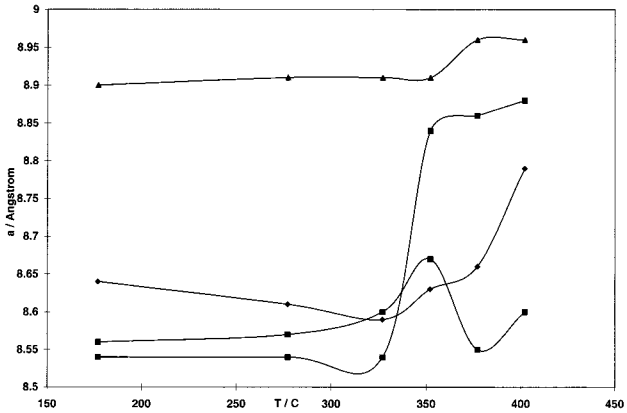

Figure 3. Change in lattice constant *a* as a function of temperature for the HBA dimer (diamonds), trimer (squares), and tetramer (triangles) cell lengths. The increase at the phase transition seen with the hexamer cell is not present for these systems. The curve for the hexamer (circles) is included for comparison purposes.

Each set of runs was repeated with different initial conditions to verify the reproducibility of the simulation schedule. No significant changes in the results discussed were found between the runs.

3. Computational Results

The calculated isobaric specific heat capacity is plotted versus simulation temperature in Figure 2 for the simulation cells studied. The value of the heat capacity is relative to 1 mol of the monomer repeat unit. All the simulation cells studied predict the temperature for the first phase transition to be in the interval 330−350 °C. The problems with these simulation cells arise with respect to the structural parameters, the graphs of which are shown in Figure 3. The main figure shows the change in lattice constant *a* for each of the simulation cells studied. Considering these, the first thing to note is that the hexamer simulation cell gives the best agreement with experiment: the lattice constant *a* changes significantly around the phase transition. The tetramer length cell gives the poorest result—there is an almost negligible change in lattice constant *a* with temperature. The dimer-length cell shows a slight change in *a* after the phase transition, although it is nowhere near as pronounced as that for the hexamer simulation cell. The trimer structure also shows a change at the phase transition, but the

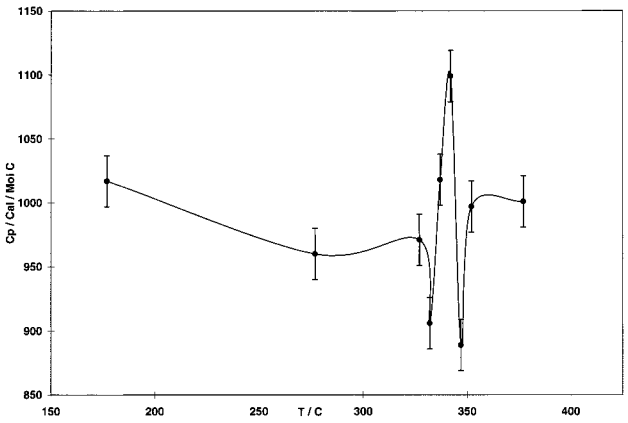

Figure 4. Calculated isobaric specific heat capacity against simulation temperature for HBA. The phase transition is seen to occur at 330−350 °C. The line is to guide the eye.

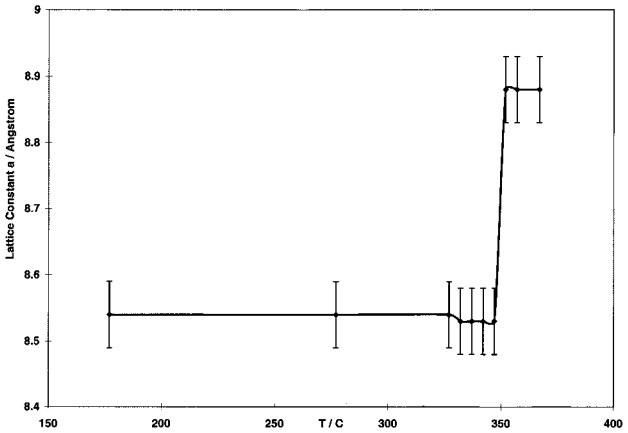

Figure 5. Change in lattice constant *a* as a function of temperature for the HBA hexamer. The increase around the phase transition found in ref 6 is seen clearly here. The line is to guide the eye.

value of *a* then *decreases* after the phase transition. This shows clearly that there are large finite-size effects associated with the smaller simulation cells (up to four monomers per chain). From these results we have chosen to study the higher-temperature phase transitions with a hexamer-length two-chain simulation cell.

HBA Phase Transition at 340 °C. The calculated isobaric specific heat capacity is plotted against simulation temperature for the HBA hexamer simulation cell in Figure 4. The variation in the calculated value of the specific heat capacity is estimated to be about ± 20 cal mol^{-1} K^{-1}. This spread in the value of C_p is obtained from five simulations on the six-monomer-length simulation cell of HBA, with identical time steps, run lengths and so forth, but with different initial conditions. Hence, the spread in values reported here may underestimate the absolute value obtained. This is particularly so for the calculation of the heat capacities which could require longer run times and larger simulation cells for a more accurate determination. However, in this work the thermodynamic quantities are only being used as a signature for the phase transitions—the nature of the transitions is extracted from the geometrical distributions. In this figure it is seen that the phase transition is calculated to occur in the range of 330−350 °C. This is in good agreement with the experimental value of 340 °C.[1,2,4,6]

The calculated lattice constants at the temperature of this phase transition are $a = 8.9$ Å, $b = 5.16$ Å, $\alpha = \beta = \gamma = 90°$. The volume is 1750 Å^3, which gives a density of $\rho = 1.36$ g/cm^3.

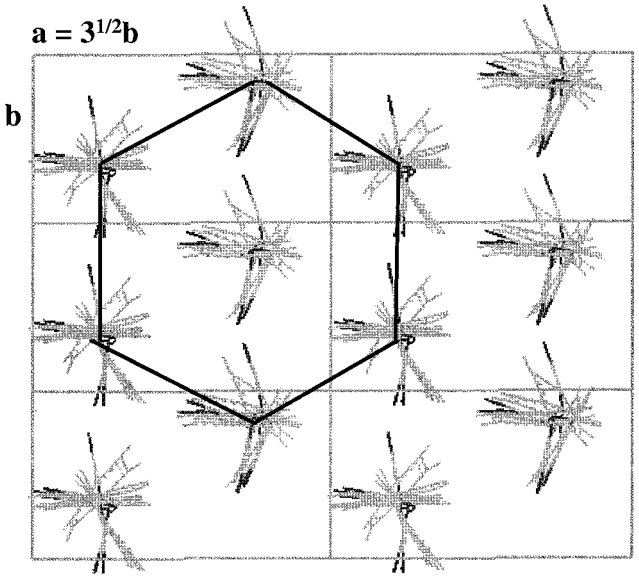

Figure 6. View of 12 HBA chains at T_{PT}, with an orthorhombic simulation cell and hexagonal packing—pseudohexagonal simulation cell.

TABLE 2: Energy of the HBA Six-Monomer Simulation Cell as a Function of γ[a]

γ/°	E^{relax}
(a)	
90	0
100	100
105	90
110	110
115	109
120	6
(b)	
90	0
100	111
105	124
110	119
115	108
120	24
(c)	
90	0
100	107
105	148
110	115
115	95
120	7

[a] All calculations are at $T = 0$ K and with the PCFF force field. E^{relax} means that the structures are relaxed orthogonal to γ. (a) Simulation cell of HBA from a temperature below the first phase transition, $T = 327$ °C. (b) Simulation cell of HBA from the temperature of the first phase transition, $T = 352$ °C. (c) Simulation cell of HBA from the temperature of the second phase transition, $T = 452$ °C.

The change in lattice constant *a* and the volume is shown in Figure 5. The absolute values of the lattice constants and the volume (and hence density) are in reasonable agreement with the experimental values. What is clearly reproduced by the simulation is the behavior of the lattice constants as a function of temperature, as discussed above. There is also a slight decrease in the value of *b* with increasing temperature. The relation $a = \sqrt{3}b$ is also seen to hold above this phase transition supporting the transformation to a pseudohexagonal chain arrangement. The orthorhombic unit cell with hexagonal packing is shown in Figure 6. However, the change from an orthorhombic unit cell ($\gamma = 90°$) to a hexagonal unit cell ($\gamma = 120°$)[12] does not take place during the time scale of the

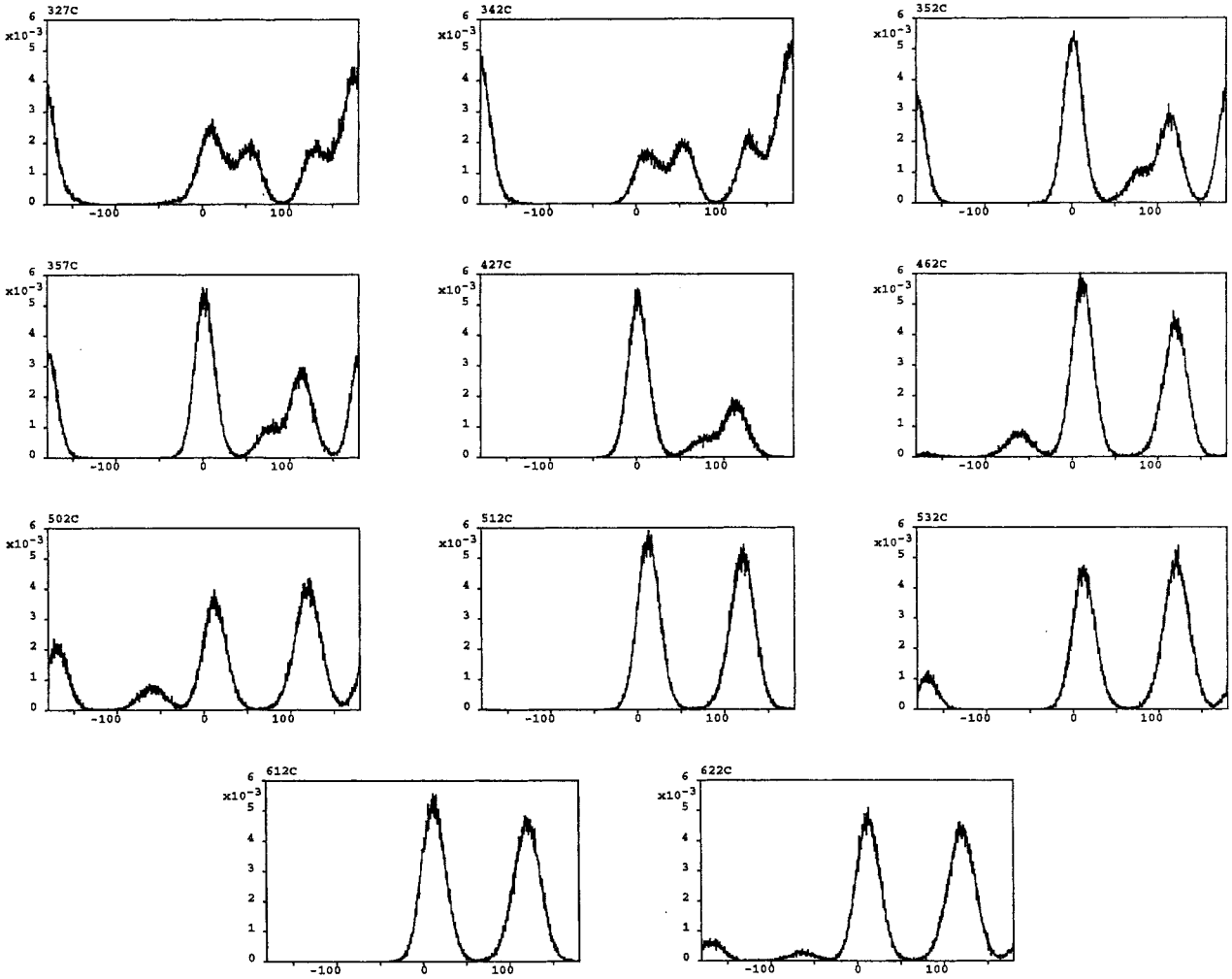

Figure 7. Torsion distribution for the E torsion shown in Figure 1. This graph shows the distribution over the temperature range studied. The temperature ranges of the phase transitions are as follows. Phase transition 1: 327−357 °C; phase transition 2: 427−502 °C; phase transition 3 and 4: 512−622 °C. The horizontal axis is the torsion angle, measured in degrees, and the vertical axis is the frequency at which each angle occurs. See text for details.

simulations. Despite this, the hexagonal structure is found to be stable above T_{PT1}. The reason HBA does not spontaneously assume a hexagonal structure with the MD simulations is presumably related to either the physical time scale of the simulations or due to particulars of the force field. It is also possible that the region of the potential energy surface needed to describe the structural transition is poorly characterized by PCFF, with the energy barrier for the transition being overestimated. Alternatively, both the orthorhombic and hexagonal structures are possibly competing structures on the free energy surface and, as indicated by these simulations, if HBA assumes one of these lattice structures it will maintain this geometry for a time-scale exceeding our simulation times.

To ascertain the stability of the orthorhombic and hexagonal structures above and below the structural transition, structures above and below the first phase transition were taken and the following procedure was carried out: the lattice constant γ was given each of the following values: 90°, 100°, 105°, 110°, 115°, and 120° and for each of these structures the system was relaxed, while constraining γ. This allows one to study the transformation from an orthorhombic unit cell to a hexagonal unit cell. However, it must be borne in mind that the energy and relaxation calculations are carried out at $T = 0$ K; thus these calculations give only an indication of the relative stability of the structures considered. The calculation shows that, above and below the phase transition, at $\gamma = 110°$, there is a large barrier for the transformation from an orthorhombic to a hexagonal unit cell, with both of these structures being local minima on the energy surface. The reason we do not see the experimentally shown transformation from an orthorhombic to hexagonal unit cell[12] can be attributed to this observation. The numerical results are shown in Table 2.

To investigate the structural changes accompanying the phase transition at 340 °C, the behavior of the torsions within the ester linkages was studied. The ester torsions are shown in Figure 1, labeled with the usual nomenclature of E, F, and G. The analysis of the torsions is carried out as follows: at a temperature below, at, and above each phase transition a distribution for each torsion, E and G, is obtained from the set of configurations generated from the dynamics simulations. No distributions are displayed for the F torsion as this shows no change over the temperature range studied.

We now discuss the results for each torsion in turn. The torsional distribution for the E torsion is shown in Figure 7. It is seen there is a significant difference in the distribution above and below the first phase transition. Below the first phase transition this torsion has maxima at 0°, 60°, 120°, and 180°. Above this phase transition the maxima now occur at 0°, 120°, and 180°, and the relative probabilities are markedly changed.

The distributions for torsion G are shown in Figure 8. Here a substantial change in the distribution at the first phase

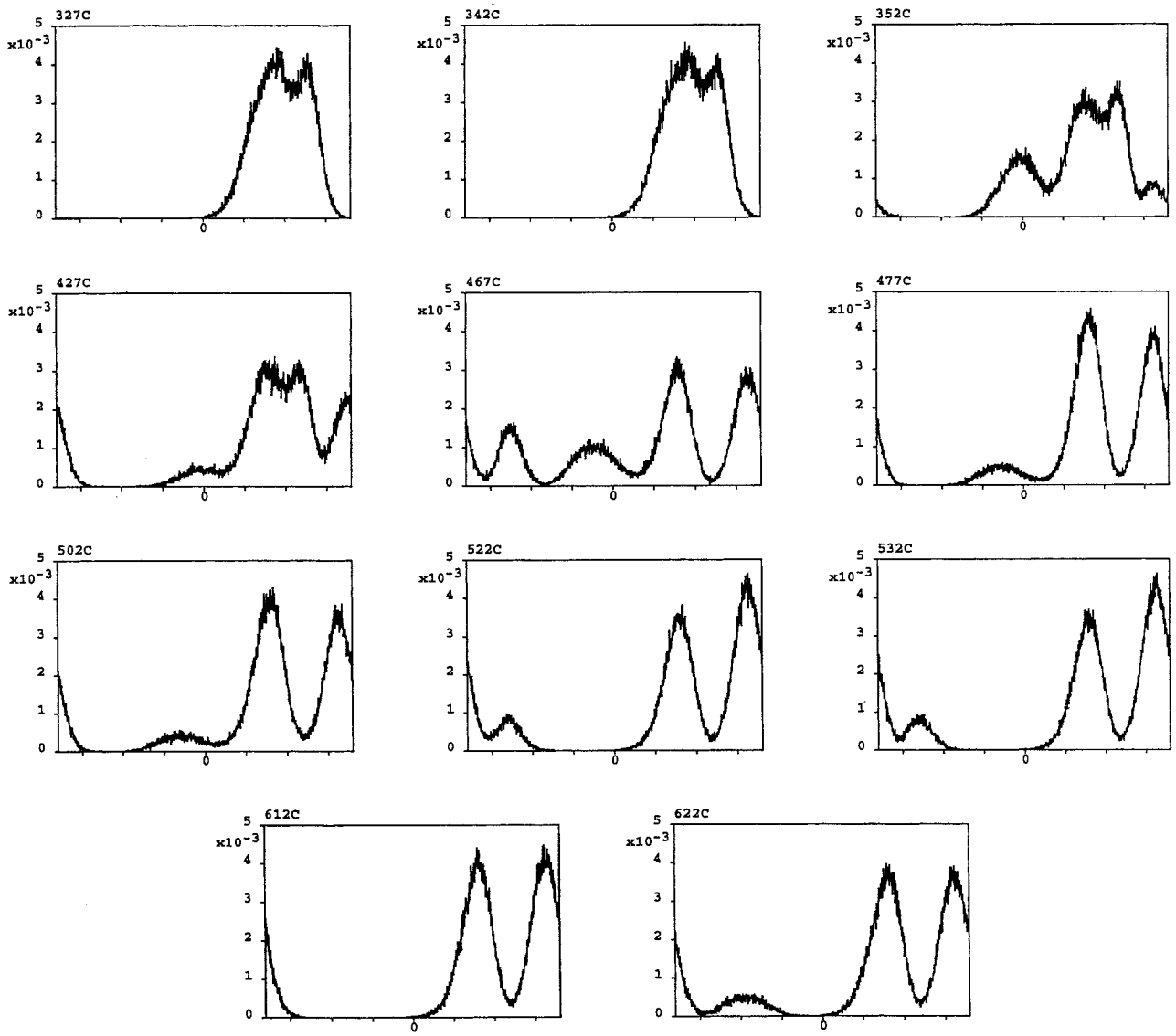

Figure 8. Torsion distribution for the G torsion shown in Figure 1. This graph shows the distribution over the temperature range studied. The temperature ranges of the phase transitions are as follows. Phase transition 1: 327−352 °C; phase transition 2: 427−502 °C; phase transitions 3 and 4: 522−622 °C. The horizontal and vertical axes are as Figure 7.

transition is seen. Below the first phase transition, we see that this torsion has complete freedom between 40° and 160°. Above the first phase transition, at 352 °C, this torsion may take on any value between 0° and 180°, with the maxima occurring at 0°, 90°, 120°, and 160°. The distributions therefore indicate that this torsion may assume a broader range of values above the first phase transition.

The plane formed by two successive phenyl rings along the chain is shown below,

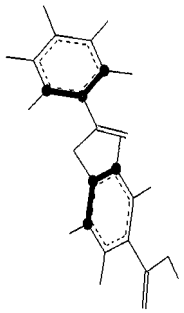

where the spheres show the atoms of interest; the corresponding distributions are shown in Figure 9. Below the first phase transition, this plane may take the values 100° or 160°. At 337 °C, this plane takes on extra freedom, which may be a pre-transition effect. Above the first phase transition the distributions show that the two phenyl rings acquire more freedom to rotate (with respect to each other). However, from the distributions the rings are never completely free to rotate. This would substantiate the conclusion of ref 5, where it was stated that the rings may rotate but do not gain complete rotational freedom. This increased rotational freedom for the rings would help explain the sharp increase in lattice constant *a* seen at this phase transition, cf. ref 3.

The torsion formed by two successive carbonyl groups along the chain is shown below,

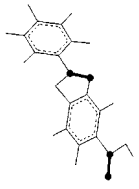

where the spheres show the atoms of interest; the corresponding

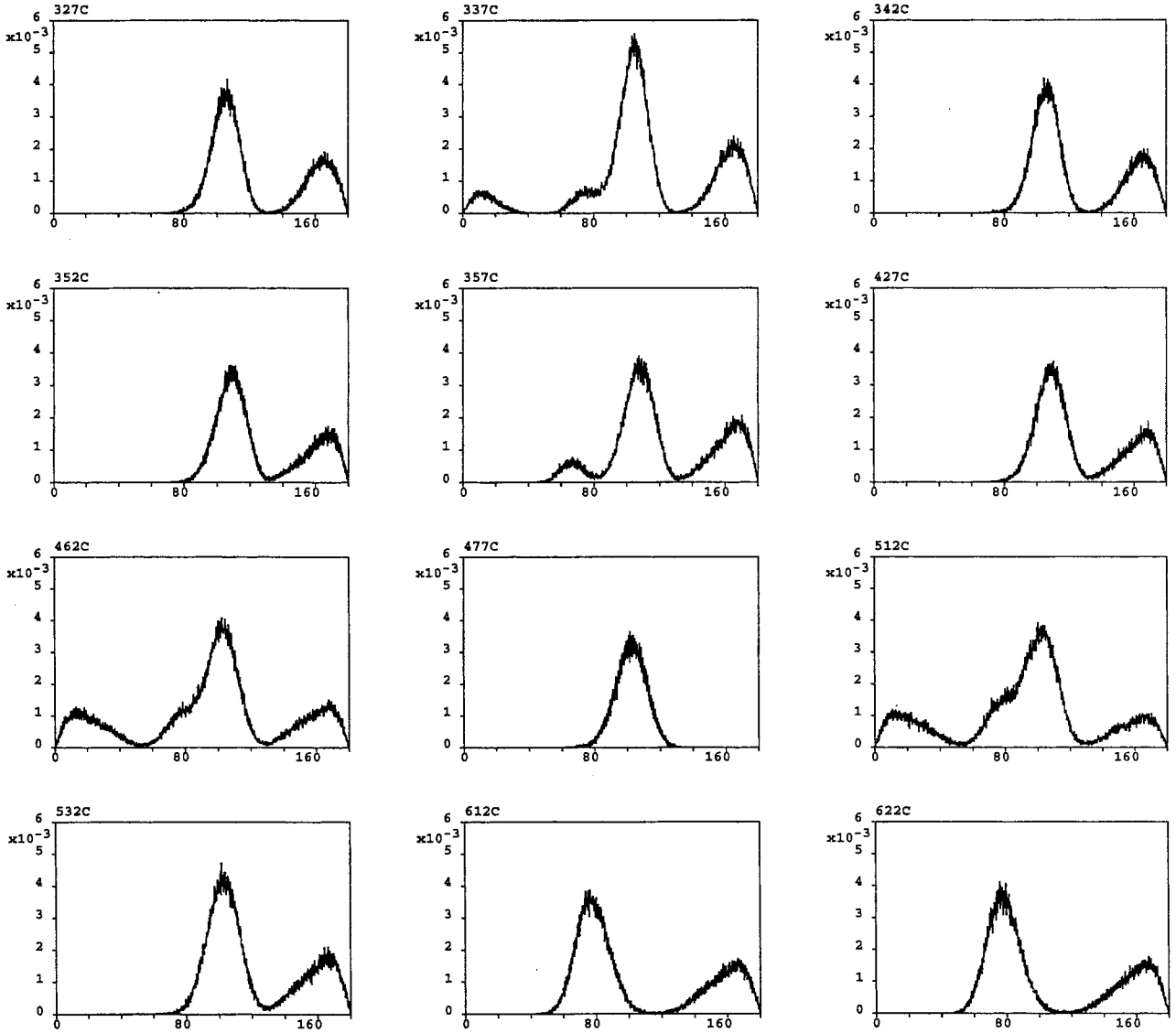

Figure 9. Distributions for the plane from two successive phenyl rings along the chain. The graph shows the distribution over the temperature range studied. The temperature ranges of the phase transitions are as follows. Phase transition 1: 327−357 °C; phase transition 2: 427−477 °C; phase transitions 3 and 4: 512−622 °C. The horizontal and vertical axes are as Figure 7.

distributions are shown in Figure 10. Below the first phase transition, the distribution for this torsion has maxima at ±60°, ±120°, and ±180°. Also, this torsion appears to be fairly free to rotate below the first phase transition. The structure is much more complicated at low temperature. What is interesting is that, at the first phase transition, this torsion *loses* some freedom and the principal angles this torsion takes on are ±60° and ±180°. This is taken to be the onset of freezing of the motion of the carbonyl groups with respect to each other.

The torsion for a carbonyl and its associated phenyl ring is shown below,

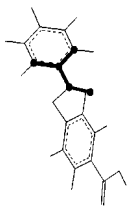

where the spheres show the atoms of interest. The distribution for this torsion is shown in Figure 11. Below the first phase transition, the distribution for this torsion shows a number of maxima. At 352 °C some of these maxima are lost. This suggests that this torsion loses some rotational freedom. It could be (from the analysis of the torsion distribution for two successive carbonyl groups) that this apparent loss of freedom is related to the freezing of the motion of the carbonyl groups.

Second Phase Transition: 430 °C. As discussed above, two possible structures were considered for the study of this phase transition. From the work of Flores et al.,[12] a hexagonal unit cell was constructed from the structure of HBA above the first phase transition. This is shown in Figure 12. The lattice constants were taken from experimental studies and are a = 9.3 Å and b = 5.3 Å. The simulations were carried out up to a temperature of 477 °C in order to examine the behavior of HBA in the vicinity of the second phase transition. The calculated isobaric specific heat capacity as a function of temperature is shown in Figure 13 a. The simulation results predict a phase transition at 430−440 °C, which is in good agreement with the experimentally measured value.[5,6]

The orthorhombic (pseudohexagonal) unit cell was taken directly from the simulations of the first phase transition. The simulations were once more carried out up to 477 °C. The lattice

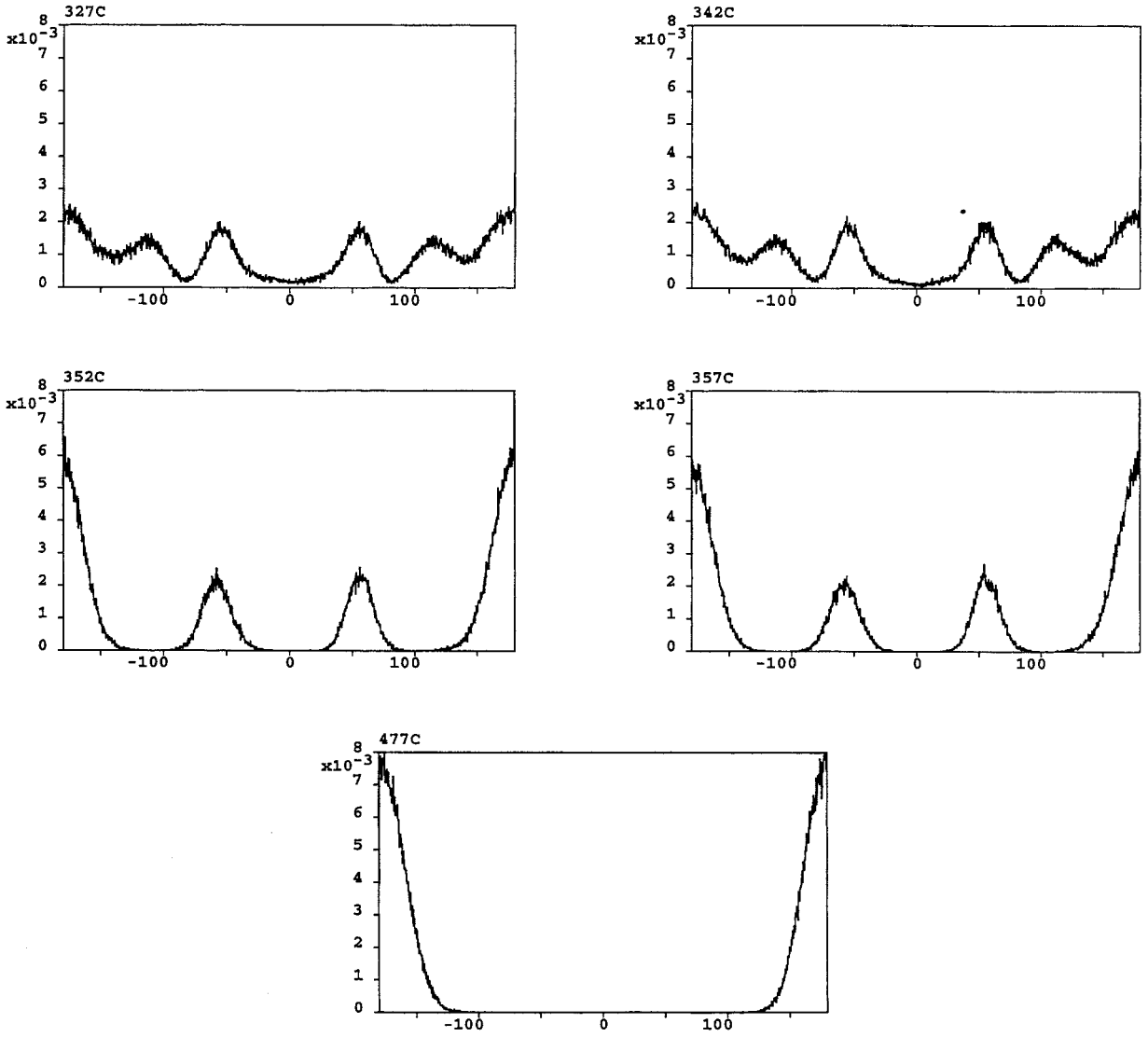

Figure 10. The distribution for the carbonyl−carbonyl torsion formed by two successive carbonyl groups along a HBA chain. The graph shows the distribution over the temperature range studied. The temperature ranges of the phase transitions are as follows. Phase transition 1: 327−357 °C; phase transition 2: 477 °C. Above 477 °C, the distribution for this torsion remains unchanged and hence no distributions at temperatures greater than 477 °C are shown. The horizontal and vertical axes are as Figure 7.

constants for this system throughout the temperature range studied are: $a = 8.83$ Å and $b = 5.19$ Å, all cell angles are 90° and the volume is 1745 Å^3. The density remains constant at $\rho = 1.37$ g/cm^3. The calculated isobaric specific heat capacity is plotted versus temperature in Figure 13b. This second phase transition is predicted to be in the range of 430−450 °C, which is in excellent agreement with the experimentally determined temperature range.

We note that the two curves of calculated specific heat capacity versus temperature are very different from each other. The unit cell with $\gamma = 120°$ gives a very broad peak, whereas that for the pseudohexagonal structure gives a very sharp, well-resolved peak. Experimentally, the endotherm at this transition is a small, wide (about 30° [6]) endotherm, which corresponds better to the curve in Figure 13a than that in Figure 13b, i.e., the structure with γ equal to 120°. The procedure outlined above for the examination of the reaction path from an orthorhombic to a hexagonal unit cell was also carried out at this phase transition. The results are very similar to those found at the first phase transition.

In what follows, the distributions are taken from the simulations of the pseudohexagonal unit cell with $\gamma = 90°$.

The distributions for the E and G torsions are shown in Figures 7 and 8, respectively. At the second phase transition both torsions loose the rotational freedom gained at the first phase transition and are only unable to undergo rotations of 90°. This behavior persists well past the temperature of this phase transition. This also suggests that a locking of motion in the chains occurs.

The distributions for the phenyl−phenyl plane are shown in Figure 9. We see clearly that above the second phase transition (462 °C), the phenyl rings experience more freedom in comparison to the first phase transition. The maxima in the distribution are at 20°, 110°, and 170°, which suggests that ring flips of 90° or 60° are occurring at this phase transition. This is in good agreement with the literature, in the sense that phenyl ring flips were suggested as the origin of this phase transition. At 477 °C, i.e., directly above the phase transition, this motion seems effectively frozen out and the rings become uniformly staggered.

The distributions between successive carbonyl groups are shown in Figure 10. This distribution is different from those below or at the first phase transition. This torsion can be between 160° and 200°, resulting in two successive carbonyl groups being planar or near-planar, but pointing in opposite direc-

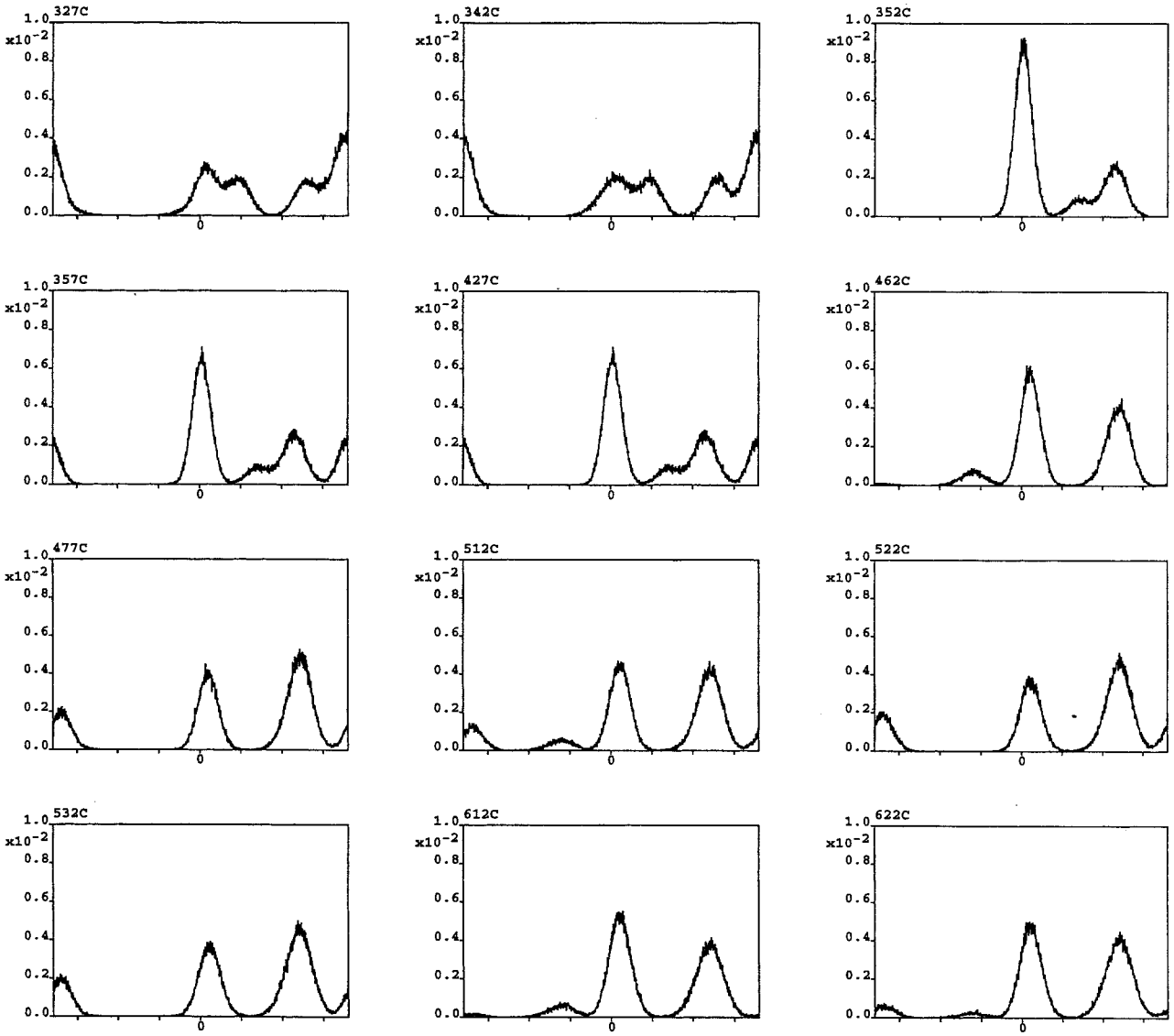

Figure 11. Distribution for the carbonyl−phenyl torsion where the carbonyl group is bonded directly to the adjacent ring. The graph shows the distribution over the temperature range studied. See text for details. The temperature ranges of the phase transitions are as follows. Phase transition 1: 327−357 °C; phase transition 2: 427−477 °C; phase transitions 3 and 4: 512−622 °C. The horizontal and vertical axes are as Figure 7.

tions. We suggest that the onset of the freezing of the motion of this torsion at the first phase transition is now complete at the second phase transition and the carbonyl groups now lock with respect to each other. This might also explain why the E and G torsions have less freedom at the second phase transition in comparison with the first phase transition. This torsion distribution persists at all temperatures studied above this phase transition.

The distribution for a carbonyl group and its associated phenyl ring is shown in Figure 11. Like the torsions discussed above, this torsion also has less freedom around the second phase transition than the first. Comparing the distributions for this torsion with those of the E and G torsions, we see that all three torsions have similar behavior. If we remember that the carbonyl groups have very little freedom to rotate, then we have to assume that it is the phenyl rings which have freedom to rotate—relative to the carbonyl groups.

All of these results indicate that the structure of *p*-HBA is much more ordered in this second phase.

High-Temperature Phase Transitions: 510−530 and 600 °C. The simulation cell above the second phase transition was relaxed for 850 ps at 457 °C and simulations were carried out up to 622 °C. The isobaric heat capacity as a function of temperature at and above the third phase transition is shown in Figure 14. This curve appears to show two phase transitions: T_{PT3} at 510−540 °C and T_{PT4} at 580−610 °C. It was previously shown that HBA decomposes around this temperature, i.e., bond-breaking occurs.[5,6] However, the quartic potential for the bond-stretching term in the PCFF force field is unable to describe dissociation processes and will not allow for decomposition. Despite this, the value of T_{PT3} is in good agreement with the work of Kricheldorf and Schwarz. The temperature at which the last phase transition occurs is also in good agreement with Jackson's reported experimental value of 610 °C. However, due to the form of the PCFF bond energy, we present these results only as an indication of the high-temperature behavior of HBA. The lattice constants are unchanged at these temperatures.

The distributions for the E and G torsions are shown in Figures 7 and 8. At the third phase transition, these torsions show no change in the values they may take. However, at 622 °C, both of these torsions take on a slightly increased range of values.

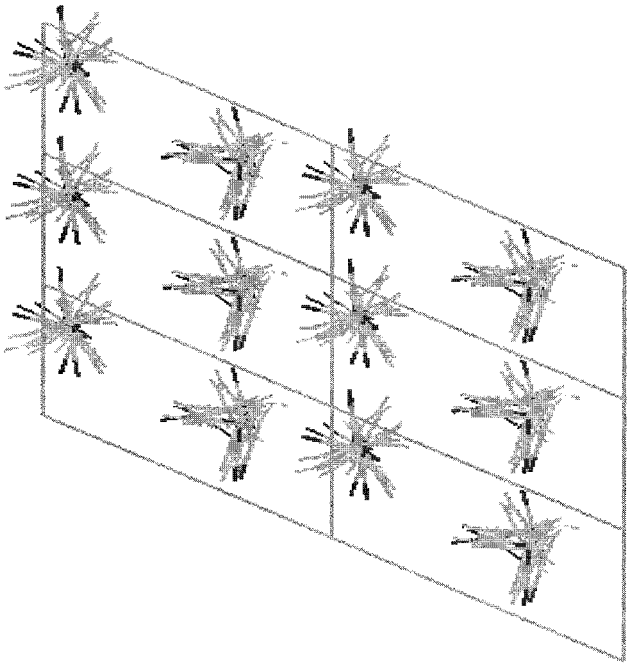

Figure 12. Hexagonal simulation cell for HBA at the first phase transition.

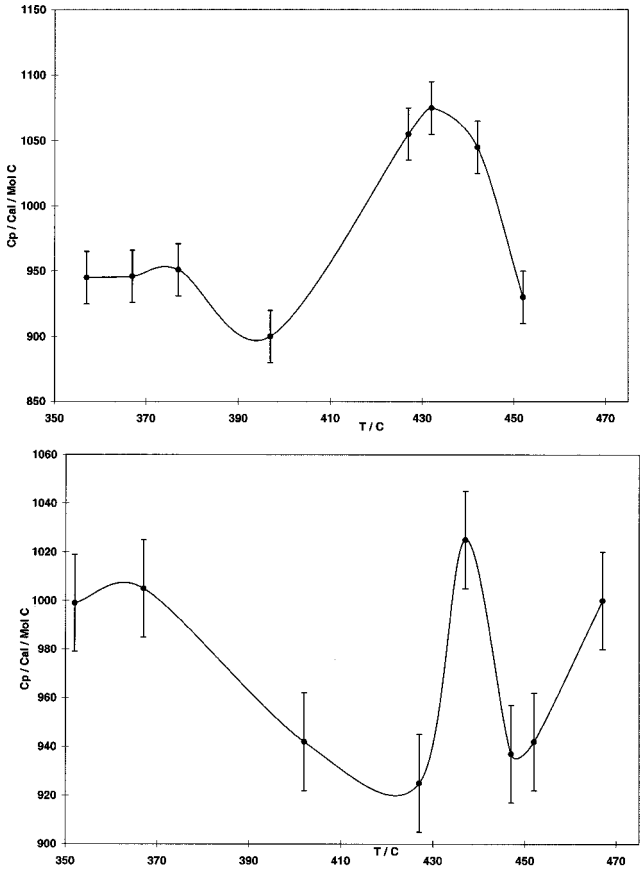

Figure 13. (a) Calculated C_p against temperature for HBA at the second phase transition with a hexagonal simulation cell, $\gamma = 120°$. T_{PT2} is calculated to be 430−450 °C. (b) Calculated C_p against temperature for HBA at the second phase transition with a pseudohexagonal simulation cell, $\gamma = 90°$. T_{PT2} is calculated to be in the range 430−450 °C.

The distribution for the phenyl−phenyl plane is shown in Figure 9. At 512 °C the rings acquire more freedom to rotate, in a manner similar to the second phase transition, which might be an explanation for the phase transition around 510−530 °C. Interestingly, at higher temperatures a distribution similar to that below the first phase transition is obtained and this seems to indicate that the rings experience no extra rotational freedom at these very high temperatures. However, we can explain this better if we assume that the rings are now unable to rotate independently of each other and that cooperative motion of the rings must occur, similar to what occurs at the second phase transition. The principal angles are 80° and 170°, suggesting ring flips of 90°.

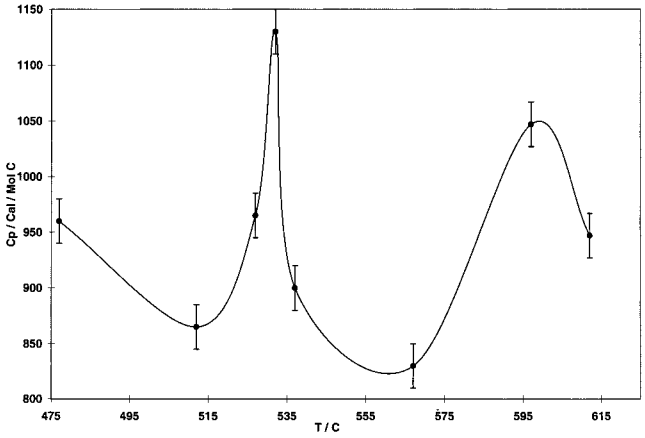

Figure 14. Calculated C_p against temperature for HBA at the third and fourth phase transitions. The phase transitions are calculated to be at 510−540 °C and 580−610 °C. See text for more details.

The distribution for the torsion between a carbonyl group and its associated phenyl ring is shown in Figure 11. This shows a little more freedom for this torsion in comparison to the distributions at temperatures slightly above the second phase transition. But, similar to the behavior of the E and G torsions, there is no significant change in the behavior of this torsion at these temperatures. The principal angles that this torsion takes are still 0° and 120°.

What then occurs at these last phase transitions, bearing in mind that the force-field used is unable to describe bond breaking? The phenyl rings seem to acquire a little more freedom to rotate (with respect to the carbonyl groups and not each other) and the E and G torsions also acquire a little more freedom to rotate. However, experimentally the very high temperatures at these last two phase transitions are enough to break bonds thus causing melting and decomposition of the sample.

4. Conclusions

Using a combination of force-field and molecular dynamics simulations we have studied the phase transitions of HBA. The simulations presented here were clearly able to predict with good accuracy the temperatures at which the phase transitions occur. The simulations were also able to model the change in lattice constant a and the volume of the unit cell at the first phase transition. The first phase transition at 340 °C appears to result in increased order along the chain axis, which is best reflected in the distribution for the carbonyl−carbonyl torsion. At the second phase transition the carbonyls have now completely locked up with respect to each other. At this point the phenyl−phenyl distributions show an increase in order along the chain axis. However this order disappears at higher temperatures. Above the second phase transition, both the E and G torsions take on only two values; those for the E torsion are 30° and 120° and those for the G torsion are 70° and 160°. The molecular motion that occurs at the phase transitions has been elucidated

and at the first phase transition the molecular motion which occurs is mainly phenyl ring motion, with an increase in freedom for the G torsion. Around the second phase transition, motion of the E and G torsions is frozen out. The phenyl rings and the carbonyl groups are no longer able to move independently of the other rings and carbonyl groups in the chain. However, the rings can move independently of the carbonyl groups and ring flip can occur. This has been clearly demonstrated in these simulations and is in agreement with previous interpretations of experimental data.

In conclusion, we have demonstrated the ability of molecular dynamics to predict the phase transitions for liquid crystal polymers containing ester linkages and to determine the molecular motion that occurs at the phase transitions. The method is currently being applied to copolymers of HBA and 1,6-hydroxynaphthoic acid.

Acknowledgment. This work was supported by the European Commission through the Brite-EuRam program, Project BE96-3615 Advanced Plastic Encapsulation (APE). M.N. acknowledges receipt of an NMRC Junior Fellowship.

References and Notes

(1) Economy, J.; Storm, R. S.; Matkovich, V. I.; Cottis, S. G.; Nowak, B. E. *J. Polym. Sci., Polym. Chem. Ed.* **1976**, *14*, 2207.
(2) Lieser, G. *J. Polym. Sci., Polym. Phys. Ed.* **1983**, *21*, 1161.
(3) Hanna, S.; Windle, A. *Polym. Commun.* **1988**, *29*, 236.
(4) Economy, J.; Volksen, W.; Viney, C.; Geiss, R.; Siemens, R.; Karis, T. *Macromolecules* **1988**, *21*, 2777.
(5) Kricheldorf, H. R.; Schwarz, G. *Polymer* **1990**, *31*, 481.
(6) Yoon, D. Y.; Masciccochi, N.; Depero, L. E.; Viney, C.; Parrish, W. *Macromolecules* **1990**, *23*, 1793.
(7) Iannelli, P.; Yoon, D. Y. *J. Polym. Sci., Part B: Polym. Phys.* **1995**, *33*, 977.
(8) Coulter, P. D.; Hanna, S.; Windle, A. *Liq. Cryst.* **1989**, *5*, 1603.
(9) (a) Sun, H.; Mumby, S. J.; Maple, J. R.; Hagler, A. T. *J. Am Chem. Soc.* **1994**, *116*, 2978. (b) Sun, H. *J. Comput. Chem.* **1994**, *15*, 752. (c) Sun, H. *Macromolecules* **1995**, *28*, 701.
(10) Allen, M. P.; Tildesley, D. *Computer Simulation of Liquids*; Clarendon Press: Oxford Science Publications, New York, 1989.
(11) van Gunsteren, W. F.; Mark A. E. *J. Chem. Phys.* **1998**, *108*, 6109.
(12) Flores, A.; Ania, F.; Balta Calleja, F. J.; Ward, I. M. *Polymer* **1993**, *34*, 2915.
(13) Jackson, J. W., Jr. *Br. Polym. J.* **1980**, *12*, 154.
(14) Huth, J.; Mosell, T.; Nicklas, K.; Sariban, A.; Brickmann, J. *J. Phys. Chem.* **1994**, *98*, 7685.
(15) Fougler, S.; Rutledge, G. C. *Macromolecules* **1995**, *28*, 7075.
(16) Rutledge, G. C. Private communication.
(17) Becke, A. D. *Phys. Rev.* **1988**, *38A*, 3098.
(18) Lee, C.; Yang, W.; Parr, R. G. *Phys. Rev.* **1988**, *37B*, 785.
(19) Harihan, P. C.; Pople, J. A. *Theor. Chim. Acta* **1973**, *28*, 213.
(20) Treutler, O.; Ahlrichs, R. *J. Chem. Phys.* **1995**, *102*, 346.
(21) Ahlrichs, R.; Baer, M.; Haeser, M.; Horn, H.; Koelmel, C. *Chem. Phys. Lett.* **1989**, *162*, 165.
(22) Computational results obtained using software programs from Molecular Simulations Inc. Dynamics simulations were done with the Cerius^2 program using the PCFF force-field. Ab initio calculations were done with the Turbomole program, and graphical displays were printed out from the Cerius^2 molecular modeling system.
(23) Parrinello, M.; Rahman, A. *J. Appl. Phys.* **1981**, *52*, 7182.
(24) Nosé, S. *J. Chem. Phys.* **1984**, *81*, 511.
(25) Hoover, W. G. *Phys. Rev.* **1985**, *A31*, 1695.
(26) Verlet, L. *Phys. Rev.* **1967**, *159*, 98.